nature nanotechnology

Supplementry information

https://doi.org/10.1038/s41565-024-01674-6

Topological valley Hall polariton condensation

In the format provided by the authors and unedited

Supplementary Information for

Topological valley Hall polariton condensation

The PDF file includes:

Supplementary Text

Figs. S1 to S6

Supplementary Text

Section I: Polariton model

The polariton dispersion was fitted using a coupled oscillator model neglecting linewidths:

$$\begin{bmatrix} E_{cav} & \Omega/2 \\ \Omega/2 & E_{ex} \end{bmatrix} \begin{bmatrix} \alpha \\ \beta \end{bmatrix} = E \begin{bmatrix} \alpha \\ \beta \end{bmatrix}.$$

Here, the cavity mode is represented as $E_{cav} = E_0 + \hbar^2 k_\parallel^2 / 2m_{cp}$ with mode energy E_0 at $k_\parallel = 0$ and effective mass m_{cp} of the cavity photon. E_{ex} is the exciton energy of the sample. E is the eigenvalue of the polaritons, and α and β represent the Hopfield coefficients satisfying $|\alpha|^2 + |\beta|^2 = 1$.

To simulate the far-field emission and the real-space polariton distribution observed in the experiment, we first consider the following differential equation:

$$E \begin{bmatrix} \psi \\ \phi \end{bmatrix} = - \begin{bmatrix} \frac{\hbar^2 \nabla^2}{2m_{cp}} & 0 \\ 0 & -\delta \end{bmatrix} \begin{bmatrix} \psi \\ \phi \end{bmatrix} + \begin{bmatrix} V & 0 \\ 0 & 0 \end{bmatrix} \begin{bmatrix} \psi \\ \phi \end{bmatrix} + \begin{bmatrix} 0 & \Omega/2 \\ \Omega/2 & 0 \end{bmatrix} \begin{bmatrix} \psi \\ \phi \end{bmatrix},$$

where ψ and ϕ are the wavefunctions for cavity photon and exciton; $m_{cp} = 0.1\, meV/(\mu m/ps)^2$ is the effective cavity photon mass; the detuning energy is $\delta = 110\ meV$; the Rabi splitting is $\Omega = 280\ meV$. The shape of the barrier is as described before, and the height is $150\ meV$. We can achieve the eigenmode in real space and eigenenergy for the system with the finite element method. The band structure in Fig. 1b was calculated with a supercell (one single cell along the x-direction and six cells on each side of the interface) shown in Fig. S2b. The polariton density distribution of the topologically protected edge state in Fig. 1c was calculated with $k_x = 2.6\ \mu m^{-1}$ and $k_y = 0$.

Then, by assuming all the eigenstates are equally distributed, the intensity of the far-field emission can be predicted by:

$$I(k, E) = \sum_{n,\kappa,\nu,\mu} \left| F_{\nu\mu}(\psi_{n,\kappa}) \right|^2 \left| \alpha_{n,\kappa} \right|^2 \Gamma_E(E, E_{n,\kappa}) \Gamma_k(k, \kappa, \nu, \mu),$$

where k is the wavevector and κ is the wavevector inside the first Brillouin zone. The terms $\psi_{n,\kappa}$, $E_{n,\kappa}$ and $\left|\alpha_{n,\kappa}\right|^2$ are the photonic part of the n_{th} eigenmode at κ, the corresponding eigenenergy and the module square of Hopfield coefficients, respectively. The functional $F_{\nu\mu}$ gives the coefficients of the Fourier transformation where $\nu(\mu)$ denotes the order of the Fourier coefficient in the reciprocal lattice direction $k_1(k_2)$. At last, the function Γ_E and Γ_k are the broadening functions in energy and wavevector:

$$\Gamma_E(E, n, \kappa) = \frac{\gamma_{n,\kappa}^2}{\left(E - E_{n,\kappa}\right)^2 + \gamma_{n,\kappa}^2}$$

$$\Gamma_k(k, \kappa, \nu, \mu) = \exp\left(-\frac{(k - \kappa - \nu k_1 - \mu k_2)^2}{\Delta(\kappa)^2} \right).$$

Where the broadening energy corresponds to the lifetime of the cavity photon with

$$\gamma_{n,k} = \frac{\hbar|\alpha_{n,k}|^2}{2\tau_{cp}}.$$

In the simulation, we assume the lifetime is $\tau_{cp} = 0.08\ ps$. For broadening in wavevector, we have

$$\Delta(k) = \Delta\left(1 - |\alpha_{n,k}|^2\right)$$

and $\Delta = 1.25\ \mu m^{-1}$ is the inverse of scattering length for excitions.

Section II: Characteristics of the valley edge state

To investigate the topological properties of the system quantitatively, we introduce the simplified Hamiltonian $H = \frac{\hbar^2\nabla^2}{2m} + V$, where m is the effective mass for the lower branch of polariton, and V is the potential determined by the cavity. With the special design of the cavity, we break the C_{3v} the symmetry of the system and lift the degeneracy at the Dirac point K and K'.

Even though the dispersions near the K and K' points are identical, they are different from each other topologically. This can be shown by calculating the valley Chern number for half of the Brillouin zone:

$$C_{K/K'} = \frac{1}{2\pi i}\int_{HBZ} dk^2\, F_{12}(k).$$

The Berry connection $A_\mu(k)$ and the associated field $F_{12}(k)$ are given by [1]:

$$A_\mu(k) = \langle\psi_n(k)|\partial_\mu|\psi_n(k)\rangle$$

$$F_{12}(k) = \partial_1 A_2(k) - \partial_2 A_1(k),$$

where $|\psi_n(k)\rangle$ is the normalized wavefunction of nth band such that it satisfies the eigenvalue problem $H|\psi_n(k)\rangle = E_n|\psi_n(k)\rangle$. The term ∂_μ is short for $\partial/\partial k_\mu$ and $\mu = 1,2$ stands for two directions on the torus.

With these definitions, we calculate the Berry curvature and valley Chern number. In Fig.S1, we show the numerically calculated Berry curvature [2]. Integrating over half of the Brillion zone for the K (K') point, we can get the valley Chern number $C_{K/K'}$. For different valley above and below the domain wall and find

$$\Delta C_{K/K'} = C_{K/K'}^{upper} - C_{K/K'}^{lower} = \pm 1.$$

According to the bulk-boundary correspondence [3], this results in a forward (backward) propagating mode near the K (K') point. On the other hand, if we reverse the configuration above and below the domain wall, the difference of valley Chern number gives $\Delta C_{K/K'} = \mp 1$. This statement can be numerically verified by the band structure shown in Fig. S1 and Fig. S2. In Fig. S2, we further confirm the field distribution of the edge state is indeed strongly localized in the domain wall between opposite valley Chern numbers.

Section III: Dynamic simulation

To simulate the transport of the valley Hall edge state and other states, we consider the Schrödinger equation as follows:

$$i\hbar\partial_t \psi = -\frac{\hbar^2\nabla^2}{2m_{pl}}\psi + V\psi$$

where ψ is the wavefunction of polariton; $m_{pl} = 0.14\, meV/(\mu m/ps)^2$ is the effective mass of exciton-polariton; the energy barrier and the potential geometry are the same as the simulations in Section I. In a near threshold approximation, we can ignore the pumping, decay, and nonlinear term. We construct a zigzag-shaped topological interface with the periodic boundary condition. By carefully choosing the initial states, we can simulate the dynamics of exciton-polariton in the cavity. Specifically, we consider three typical initial states:

1. The normal state: we consider the following Gaussian shape initial wavefunction:

$$\psi_0 = \Psi \times Exp\left[-\frac{x^2+y^2}{\Delta^2}\right]$$

Where $\Delta = 3$ in the unit of lattice constant in the simulation. The Ψ is the superposition of all eigenstates with $k_x = k_y = 0$. The wavefunction only spreads instead of propagating along the edge. (Supplementary Video 1.mp4)

2. The topological valley Hall edge state: To see the evolution of the edge state, we first find the stationary state of the system with periodic boundary conditions in the x-direction. We choose the eigenstate inside of the gap and denote it as ψ_{ini} (blue star in Fig. S6). Notice ψ_{ini} is infinite in the x-direction, we must truncate it before we put it into the Z-shaped system. This is done by assuming the initial wavefunction is a Gaussian wave packet:

$$\psi_0 = \psi_{ini} \times Exp\left[-\frac{x^2}{\Delta^2}\right]$$

Where $\Delta = 2\sqrt{6}$ in the unit of lattice constant in the simulation. With such an initial condition, we can see that the topological edge state transport on the topological interface barely feels backscattering from the corners. (Supplementary Video 2.mp4)

3. The backscattering of the non-topological edge state: Choosing the ψ_{ini} state just above the topological gap state (green star in Fig S6) with the initial condition:

$$\psi_0 = \psi_{ini} \times Exp\left[-\frac{x^2}{\Delta^2}\right]$$

We find strong backscattering when the wavefunction hits the corner (Supplementary Video 3.mp4), since the state is above the topological bandgap and does not have the topological protection.

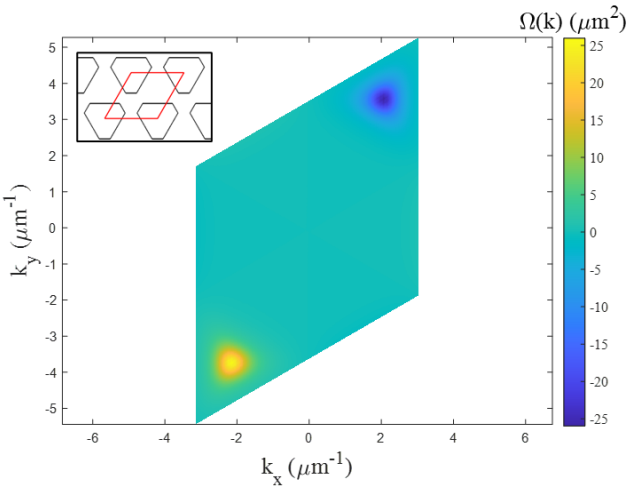

Supplementary Fig. 1| The Berry curvature result for the bulk state. The inserted picture shows the configuration of the bulk area. The red quadrilateral in the inset represents the unit cell.

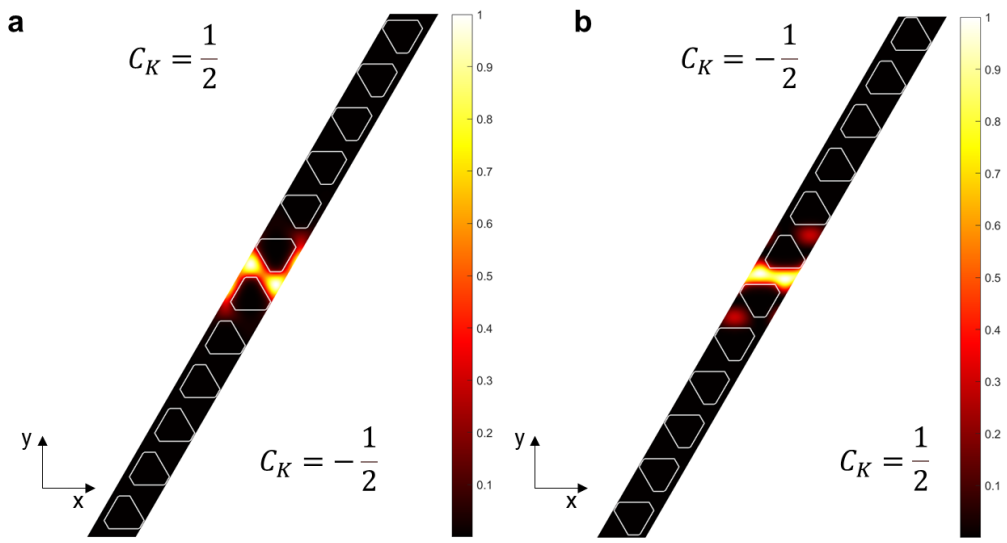

Supplementary Fig. 2| The distribution of the edge state near the *K* point. The states are well localized near the edge. In the left panel **a**, the configuration of the potential above the domain wall gives $C_K = \frac{1}{2}$ in the bulk state. Below the domain wall, the potential configuration (which is obtained by rotating the upper one by 180°) gives $C_K = -\frac{1}{2}$ in the bulk state. Thus, we get $\Delta C_K = 1$, which gives a forward (right) propagating edge state. In the right panel **b**, we have an opposite configuration which gives a backward (left) propagating state near the K point.

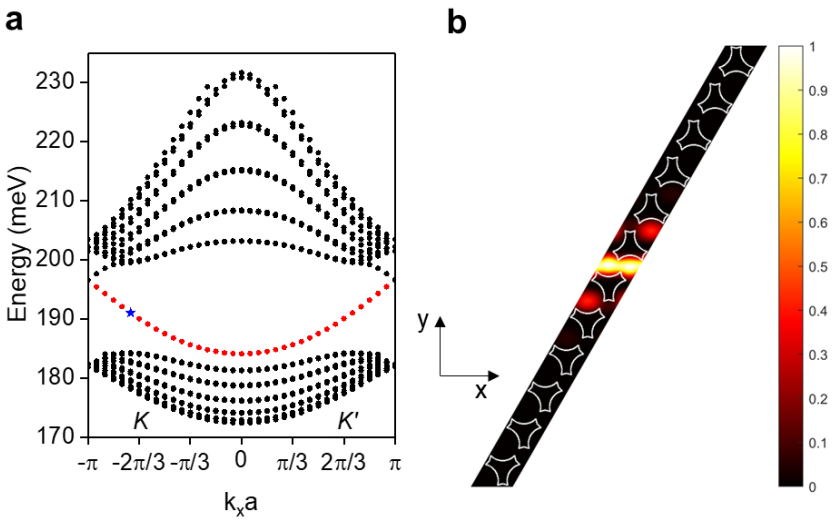

Supplementary Fig. 3| The topological edge state of the polariton valley Hall insulator with the design of coupled micropillars. a, Projected band structure of the topological interface in a supercell finite in the y direction. The topologically protected valley edge states are confined to the interface, as indicated by the solid red dots. The lattice period is a = 1.2 μm, and the diameters of the large and small pillars are 0.95 and 0.51 μm, respectively. **b**, The real-space polariton density distribution of the topologically-protected edge state corresponding to the state marked by a blue star in a.

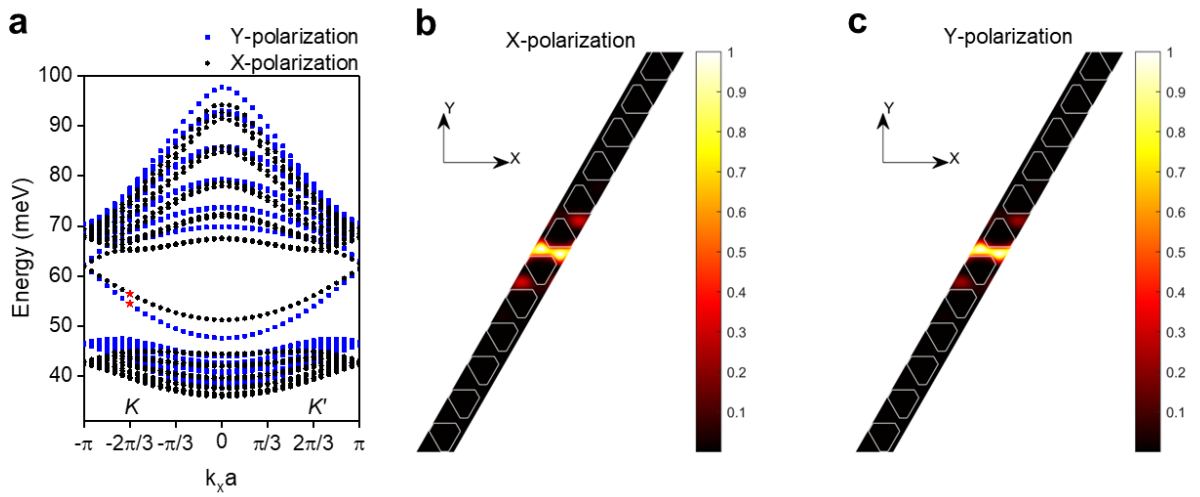

Supplementary Fig. 4| The calculated energy band and polariton distributions of the valley edge state with a $CsPbBr_3$ optical birefringence. Due to the birefringence, the widely used $CsPbBr_3$ cavity has two linear polarized polariton branches. The two orthogonally polarized polariton branches exhibit an energy splitting of ~8 meV [4]. Panel a shows the projected band structure of the topological interface in a supercell that is finite in the y direction. The in-plane anisotropy was described with a photon effective mass tensor along the x and y axis as $[m_{xx}, m_{xy}; m_{yx}, m_{yy}] = [1.12\, m_{cp}, 0.88\, m_{cp}; 0.88\, m_{cp}, 1.12\, m_{cp}]$, where $m_{cp} = 0.1\, meV/(\mu m/ps)^2$ is the effective cavity photon mass without birefringence. m_{xy} represents the effective mass of the x polarization along the y-axis. For the topological interface along the x-axis, there are two sets of energy bands with x and y polarization, as shown in a. The edge states with x and y polarizations have different energies (red stars in **a**) and real-space distributions (**b** and **c**). For the topological boundary structure with a 120° sharp corner described in our manuscript, the in-plane refractive index tensors on the two edges are different, leading to distinct eigenstates. Consequently, when a topological edge state propagates across the 120° sharp corner, backscattering occurs because of the energy discontinuity.

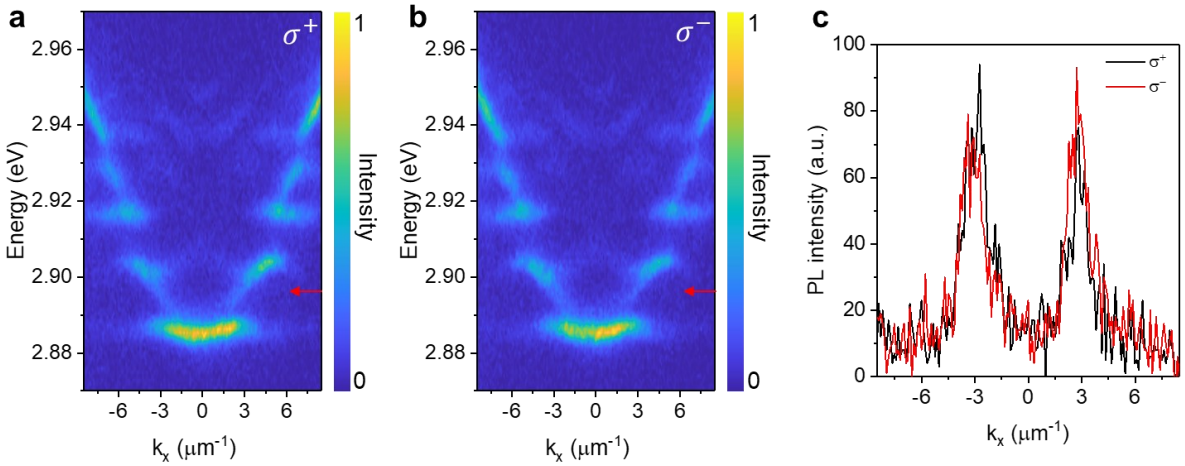

Supplementary Fig. 5| The circular polarization-resolved momentum-space PL dispersions. **a** and **b**, left and right-circular polarized PL dispersions of the topological interface along the x-axis, respectively. **c**, the line cut plots of the PL at 2.896 eV in **a** and **b**. Here, no obvious asymmetry between left- and right-circular polarizations was observed. Due to the lack of photon spin degree of freedom, no spin-valley locking was observed in our perovskite microcavity.

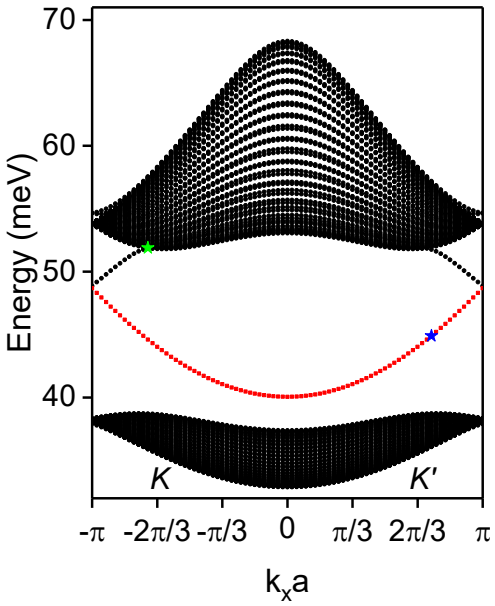

Supplementary Fig. 6| The topological edge state of the polariton valley Hall insulator for the dynamic simulation. The blue and the green stars represent the initial state of the topological and the backscattering non-topological edge state, respectively. Due to the use of a simplified model that only considers the lower polariton branch, larger effective mass parameters were employed, resulting in slight differences in the band structure compared to Fig. 1 in the main text.

References:

1. Fukui, T., Hatsugai, Y. & Suzuki, H. Chern numbers in discretized Brillouin zone: Efficient method of computing (spin) Hall conductances. *J. Phys. Soc. Japan* **74**, 1674–1677 (2005).
2. Asbóth, J. K., Oroszlány, L. & Pályi, A. A Short Course on Topological Insulators. *Lect. Notes Phys.* **919**, 166 (2016).
3. Hasan, M. Z. & Kane, C. L. Colloquium: Topological insulators. *Rev. Mod. Phys.* **82**, 3045–3067 (2010).
4. Peng, K. *et al.* Room-temperature polariton quantum fluids in halide perovskites. *Nat. Commun.* **13**, 7388 (2022).